



Influence of sulfurization time and Cu-ZnS-Sn stack order on the properties of thermally evaporated CZTS thin films

Nagabhushan Jnaneshwar Choudhari¹, Sajjan D. George², and Y. Raviprakash^{1,*}

¹ Semiconductors and Photovoltaics Lab, Department of Physics, Manipal Institute of Technology, Manipal Academy of Higher Education, Manipal 576104, India

² Centre for Applied Nanosciences, Department of Atomic and Molecular Physics, Manipal Academy of Higher Education, Manipal 576104, India

Received: 25 November 2021

Accepted: 4 January 2022

Published online:
21 January 2022

© The Author(s) 2022

ABSTRACT

Cu₂ZnSnS₄ (CZTS) thin films were synthesized in a two-step procedure. Sulfurization of stacked thin films SLG/ZnS/Sn/Cu (S1) and SLG/Cu/Sn/ZnS (S2) after sequential deposition of Cu, ZnS, and Sn precursors was carried out. At 550 °C, two sulfurization periods were applied to both stack orders. Sample S1 sulfurized for 30 min (S1-T30) had a better crystallite size of roughly 50 nm, lower lattice strain, and lower dislocation density than other samples. The Cu/Zn cation ordering in the CZTS crystal system was significantly affected by stack sequence and sulfurization time, according to Q-factor calculation. The stack order of the S1 series allowed for homogenous and distinct particle development. From the elemental analysis, it is observed that the stack sequence and sulfurization used for sample S1-T30 permitted a near stoichiometric composition. The sample S1-T30 exhibited an optimal band gap value of 1.47 eV. To propose feasible alterations in the structural ordering, band gap calculations were used. In comparison to the stack order of the S2 series, the stack order SLG/ZnS/Sn/Cu with a sulfurization time of 30 min created a single-phase CZTS, implying less synthesis time to obtain an absorber quality CZTS layer for solar photovoltaic application.

1 Introduction

The current photovoltaic market is heavily dominated by silicon-based solar cells. However, materials like cadmium telluride (CdTe) and copper indium

gallium diselenide (CIGS) have been gaining an increasing portion of the photovoltaic (PV) market as a result of developments in thin-film technology. The emerging popularity of these materials can be attributed to the comparable power conversion

Address correspondence to E-mail: raviprakash.y@manipal.edu

efficiency to silicon-based photovoltaic cells but at a reduced cost and with far less material consumption [1]. The discovery of earth-abundant, non-toxic, and low-cost chalcogenide kesterite materials originated from the hunt for material to reduce costs even further and to replace the poisonous and rare components used in existing thin-film PV. The maximum power conversion efficiency attained so far is 11% for CZTS (Copper Zinc Tin Sulfide) and 12.6% for CZTSSe (Copper Zinc Tin Sulfo-Selenide), indicating that there is still space for improvement [2]. Current thin-film PV technologies, such as CdTe and CIGS, face a major scarcity of material issues to satisfy future energy demands at a terawatt (TW) scale [2, 3]. CZTS appears as a solution, giving a more cost-effective thin-film absorber material. The main motivation for continued research in kesterites is its complexity, structure richness, and tunability with several reported alloying and doping [4].

Various researchers have studied the stack order effect on the properties of CZTS/Se thin films. Multiple thin-film coating methods have been employed such as thermal evaporation, sputtering, and spray pyrolysis to obtain CZTS thin films [5–7]. Fairbrother et al. studied the stacking order effect on the optoelectronic properties of CZTSe thin films deposited by magnetron sputtering [8]. Avendaño et al. used binary metal sulfide stack layers to obtain phase pure CZTS thin films by electrodeposition technique [9]. Thota et al. utilized sequential sputtering to deposit different stacks of elemental precursors to obtain phase pure, homogeneous CZTS thin films. Phase evolution and metal decomposition dependency on the stack order were studied [10]. Lee et al. studied the effect of elemental precursor stack and alloy precursor stack on the optoelectronic properties of CZTSe thin films [11].

The present study aims at understanding the impact of sulfurization time and stack order effect on the Cu/Zn cation ordering of CZTS thin films. Herein, we explore the extent of the effect of the above-mentioned preparatory parameters on the structure ordering of CZTS thin films by utilizing the structure, composition, morphology, and band gap studies.

2 Experimental details

Vacuum thermal evaporation technique was employed to deposit CZTS thin films. Soda-lime glass (SLG) was used as a substrate. Before the deposition standard cleaning procedures were followed as mentioned in our previous work [7]. High-purity elemental [Cu (99.999%), Sn (99.9985%)], and compound precursors [ZnS (99.995%)] along with cleaned SLG substrates were loaded into the thermal evaporation chamber. The base pressure of the chamber was maintained at 4×10^{-6} mbar with liquid nitrogen assistance. In this work, a two-step CZTS thin-film synthesis was followed: Sequential evaporation of precursors and Sulfurization of deposited thin films.

Two types of stacked CZTS thin films were deposited, namely, (a) SLG/ZnS/Sn/Cu and (b) SLG/Cu/Sn/ZnS, and resulting thin films were categorized into S1 and S2 series. The Sn was intentionally sandwiched between Cu and ZnS layers to reduce its substantial decomposition during sulfurization reaction. The stacked CZTS thin films were subjected to sulfurization. Sulfurization setup details and the process conditions are mentioned in our previous report [7]. The sulfurization temperature was set at 550 °C at Zone 2. Temperature rate profiles were named T30 and T60. Figure 1 shows the ramp-soak cycles followed for the S1 and S2 samples series. Sample with stack order S1 and sulfurization time of 30 min at 550 °C is termed as S1-T30 and sample with stack order S1 and sulfurization time of 60 min at 550 °C is termed as S1-T60. Similar sample naming was followed for the S2 series.

Structural information was obtained using X-ray diffraction with Cu-K α radiation ($\lambda = 1.5405 \text{ \AA}$, $I = 15 \text{ mA}$, $V = 40 \text{ kV}$, and $2\theta = 10^\circ\text{--}80^\circ$) (Rigaku Miniflex 600). A Raman spectrometer with a near-resonant excitation wavelength of 785 nm with a laser power of 34 mW was used (B&W TEK i-Raman Plus Spectrometer). Compositional data were obtained using energy-dispersive spectroscopy probe at an acceleration voltage of 15 kV (EDS) and surface morphology was acquired using a scanning electron microscope at 5 kV acceleration voltage (Zeiss EVO MA18 with Oxford EDS INCA X-act). UV-Visible spectrophotometer was used to acquire the absorption spectra (Scan range 190–1100 nm) (Shimadzu 1800 UV).

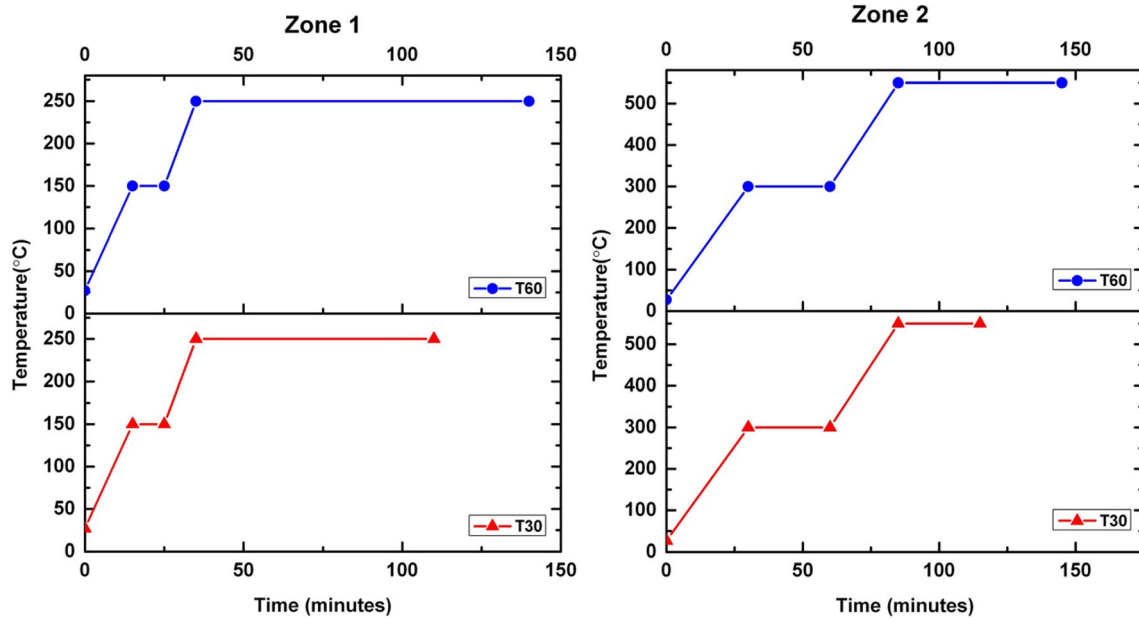


Fig. 1 Ramp-soak cycles followed at zone 1 and zone 2 for S1 and S2 series

3 Results and discussion

3.1 Structural analysis

X-ray diffractogram of CZTS thin films for two different soak profiles are shown in Fig. 2. Sample S1-T30 shows the formation of single-phase CZTS. After subjecting the as-deposited thin films to sulfurization, significant improvements in the structural properties of CZTS thin films were observed. The diffraction peaks for all the samples corresponding to the (112), (200), (220), (312), (008), (224), and (332) planes are in line with the reported values (JCPDS No. 26-0575) which confirm the formation of CZTS [12–14]. All samples show predominant orientation along (112) crystallographic plane. The lattice parameter is computed using formula [15]:

$$\frac{1}{d^2} = \left(\frac{h^2 + k^2}{a^2} \right) + \frac{l^2}{c^2}, \tag{1}$$

where h, k and l are miller indices and d is the interplanar spacing.

The crystallite size (D) is calculated using Scherrer's equation [16]:

$$D = \frac{0.9 \lambda}{\beta \cos \theta}. \tag{2}$$

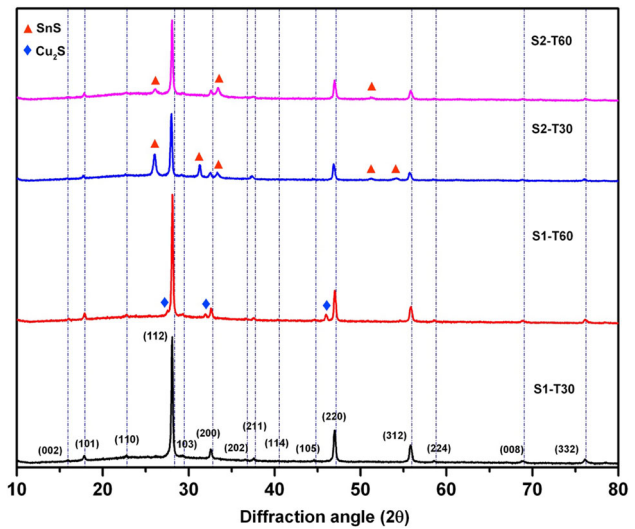


Fig. 2 X-ray diffractograms of samples S1-T30, S1-T60, S2-T30, and S2-T60 CZTS thin films

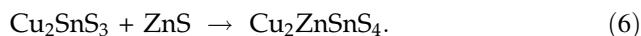
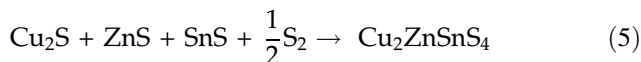
The obtained value is in the range of 41–50 nm. Equations utilized to calculate lattice strain (ϵ) and dislocation density (δ) are as follows [17]:

$$\beta \cos \theta = \frac{0.9 \lambda}{D} + 4 \epsilon \sin \theta \tag{3}$$

$$\delta = \frac{1}{D^2}. \tag{4}$$

Calculated structural parameters are tabulated in Table 1. From Fig. 1, it can be noted that except for

S1-T30, all other samples showed the formation of secondary phases. Sample S1-T60 showed Cu₂S secondary phases at 31.98°, 45.98°, and 54.58° [18, 19]. In the samples S2-T30 and S2-T60, secondary phases formed were of the SnS phase with peak positions at 26.12°, 31.28°, 33.32°, 51.24°, and 54.16° [20, 21]. From Table 1, it is evident that crystallite size was largest (50 nm) for the sample with SLG/ZnS/Sn/Cu stack order and sulfurized for 30 min at 550 °C. The other sample of the S1 series which was sulfurized for 60 min showed decreased lattice strain and dislocation density. Contrary to the S1 series, samples in the S2 series improved with the increase in the sulfurization time which in turn reduced the intensity of the secondary phases (see Fig. 3). This might be because of the ZnS top layer. ZnS has a higher melting point compared to the other two precursors employed. This makes the ZnS layer act as a thermally insulating layer which does not let the multi-level reaction complete leading to the formation of the secondary phases. The proposed reaction pathway for the formation of the CZTS layer is shown below [22].



The changes in the lattice parameter 'c' can be assigned to the order–disorder transition. The increment in the value of 'c' indicates a possible decrement in the structural ordering [23]. In the present work, the lattice parameter 'c' increased from 10.84 Å for S1-T30 to 10.90 Å for S2-T60, suggesting a decreased ordering and increased Cu/Zn antisites.

3.2 Raman analysis

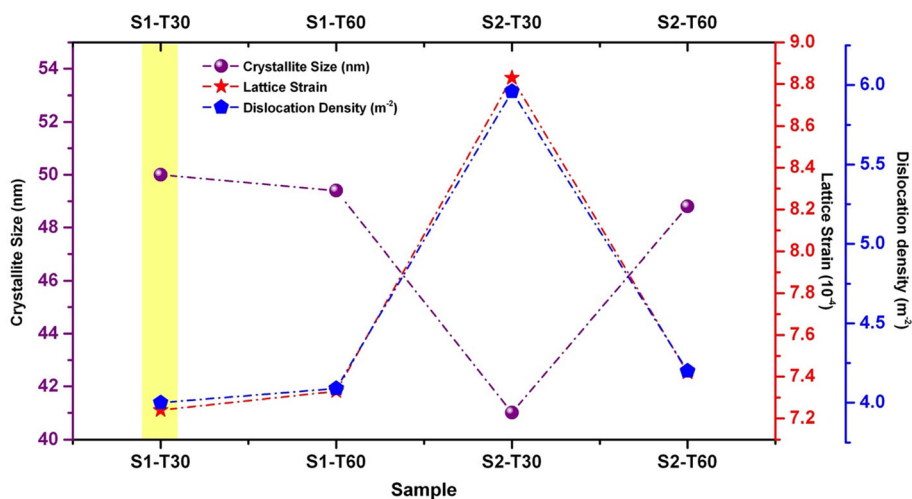
Near-resonant Raman spectroscopy was employed to study the relation of structural ordering with the stacking sequence and sulfurization time. The instrumental resolution in the Raman measurement was around 4 cm⁻¹. Figure 4 shows the deconvoluted Raman spectra utilizing an excitation wavelength of 785 nm. Peaks were deconvoluted using the Lorentzian peak fitting function. Being very sensitive to small band gap fluctuations, near-resonant measurement helps in understanding the Cu/Zn cation ordering. All the samples showed peaks around 261 cm⁻¹, 284 cm⁻¹, 302 cm⁻¹, 335 cm⁻¹, 363 cm⁻¹, and 372 cm⁻¹ which agree with the existing literature [24, 25].

To measure the Cu/Zn cation ordering associated with the variation in the stack arrangement and sulfurization time, a unitless quantity called Q-factor has to be calculated. This is calculated by taking the ratio of the intensity of m_{2A} and m_{3A} ($Q = I(m_{2A})/I(m_{3A})$) related to peaks at 284 cm⁻¹ and 302 cm⁻¹, respectively. The more the Q-factor value, the less is the structural disorder or in other terms, more is the Cu/Zn ordering. The higher Q-factor indicates the reduced randomness in the occupation of the Zn site by Cu or vice versa which is also termed as antisite defect [26]. The term m_{1A} refers to the main vibrational peak around 335 cm⁻¹. As shown in Table 2, the Q-factor is highest, i.e., 9.18 and the FWHM is the lowest, i.e., 7.63 cm⁻¹ for the S1-T30 sample. This suggests the reduction in the structural disorder or antisite defect and increased crystallinity of the sample, respectively. The Q-factor and FWHM have decreased steadily after the S1-T30 sample as seen in Table 2, which is in correlation with the XRD

Table 1 X-ray diffraction data of S1-T30, S1-T60, S2-T30, and S2-T60 CZTS thin films

Sample	Crystallite size (nm)	d spacing (Å)	Lattice Parameter		Volume (Å ³)	c/2a ratio	Lattice strain (10 ⁻⁴)	Dislocation density × 10 ¹⁴ (m ⁻²)
			a (Å)	c (Å)				
S1-T30	50	3.17	5.46	10.84	324.07	0.992	7.24	4.00
S1-T60	49	3.17	5.46	10.89	325.13	0.997	7.33	4.09
S2-T30	41	3.18	5.47	10.90	327.38	0.996	8.83	5.96
S2-T60	49	3.17	5.46	10.90	326.07	0.998	7.42	4.20

Fig. 3 The plot of crystallite size, lattice strain, and dislocation density for S1 and S2 series sulfurized at different sulfurization times



analysis, suggesting the reduction in the structural ordering (Cu/Zn cation order)/increased antisite defects in the crystal system (see Fig. 5).

3.3 Compositional and morphological analysis

The chemical composition of the synthesized thin films is compared with the atomic stoichiometry of Cu (25%), Zn (12.5%), Sn (12.5%), and S (50%) and is tabulated in Table 3. Figure 6 depicts the composition of the CZTS thin films for various samples. As it is seen from the table, out of all the samples, the S1-T30 sample shows a good composition compared to other samples. From the elemental composition, it is evident that the Cu_2S is predominant in the S1-T60 sample which is in line with the XRD analysis. In the case of the S2 series, copper was increased and zinc was decreased with increased sulfurization time during which tin and sulfur remained the same without much variation leading to the formation of the SnS secondary phase. Figure 7 shows the EDS spectrum of the S1-T30 sample.

Figure 8 shows SEM analysis of microstructures of stacked and sulfurized CZTS thin films. Morphology suggests continuous thin films. Considerable variations in the stacked and sulfurized thin films are evident from the SEM micrographs. The seen dominant CZTS growth in the S1-T30 sample changed to a dominant Cu_2S growth in S1-T60. The observed large particles on the surface in Fig. 9d are of Cu_2S particles. In the case of the S2 series, there is a decrement in the particle size with the increase of sulfurization time from 30 to 60 min results in increased grain

boundaries posing a resistance for the flow of electrons.

3.4 UV-Vis analysis: band gap measurement

Optical spectra of sulfurized thin films were acquired in the range of 190–1100 nm. To estimate the band gap, Tauc's relation was used [27, 28]. Estimation of band gap was done by extrapolating the tangent drawn from the linear region of the graph to the x -axis. Figure 10 shows the estimated band gap of the prepared samples. The band gap values obtained between 1.44 and 1.47 eV are in line with the reported values [29]. Literature suggests that the variation in the band gap can be attributed to the Cu/Zn antisite disorder [23, 30]. The decrease in the band gap energy from 1.47 to 1.31 eV suggests the possible degradation in the order parameter which is in line with the X-ray diffraction analysis and Raman analysis. It can be mentioned that the sample with 1.47 eV is more structurally ordered than the sample with a band gap of 1.31 eV. The band gap of samples S2-T30 shows a decreased band gap of 1.31 eV. This may be due to the significant presence of SnS secondary phases along with the CZTS phase.

4 Conclusion

CZTS thin films were prepared by utilizing two different stacking sequences, namely, SLG/ZnS/Sn/Cu (S1) and SLG/Cu/Sn/ZnS (S2) using the sequential evaporation method. The impact of sulfurization time

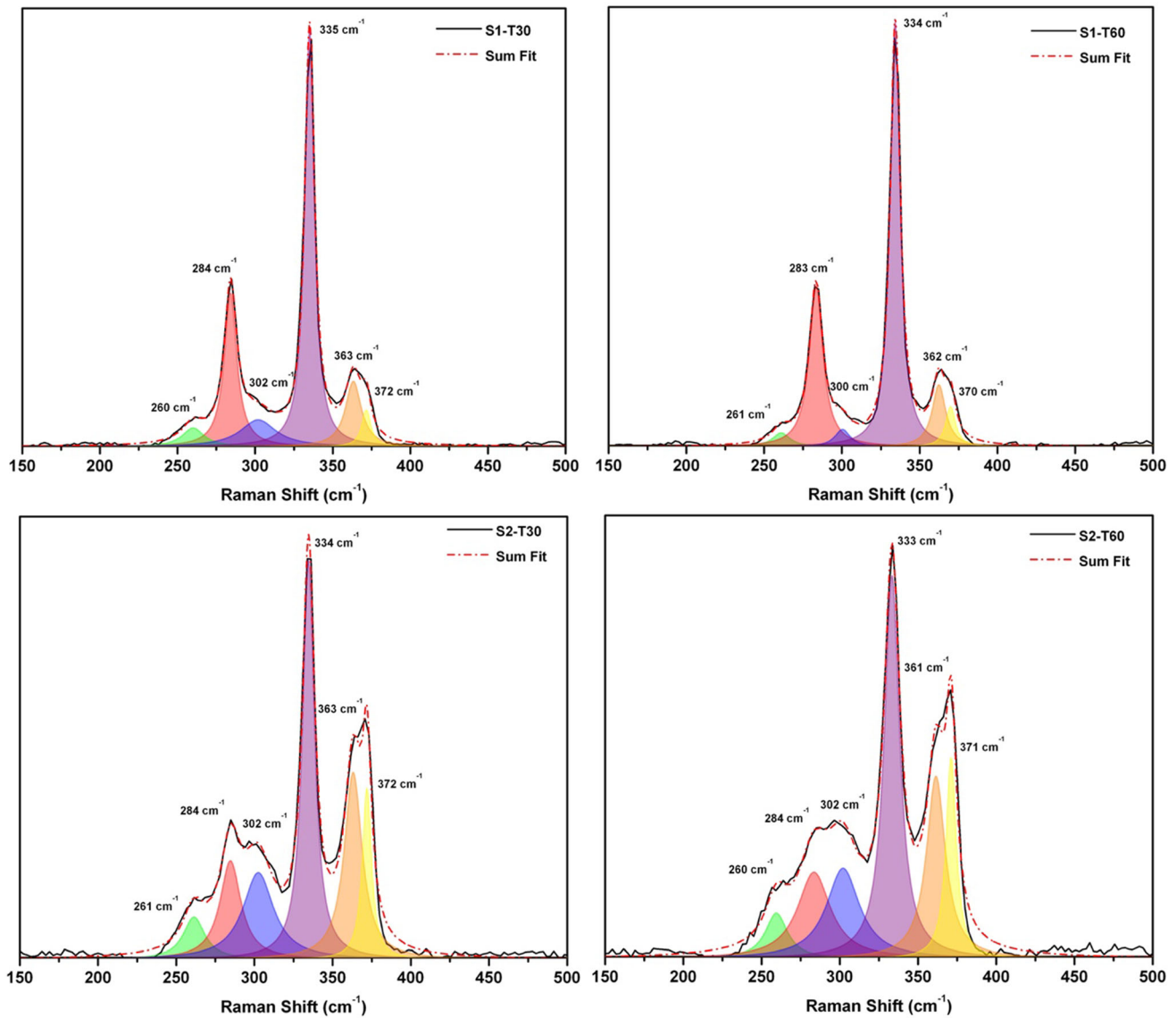


Fig. 4 Individual plots of deconvoluted Raman spectra of CZTS thin films with Lorentzian peak fitting function

Table 2 Q-factor and FWHM of CZTS thin films

Sample	$Q = I(m_{2A})/I(m_{3A})$	m_{1A} FWHM (cm^{-1})
S1-T30	9.18	7.63
S1-T60	5.69	7.84
S2-T30	1.13	9.26
S2-T60	0.95	11.93

and stack arrangement on sequentially evaporated CZTS thin films was explored. X-ray diffraction analysis showed that sample S1-T30 was of a single phase and more structurally ordered. Raman analysis suggested the increasing Cu/Zn antisite disorder after the S1-T30 sample. Elemental homogeneity and near stoichiometric composition were found for the S1-T30 films. The formation of secondary phases and

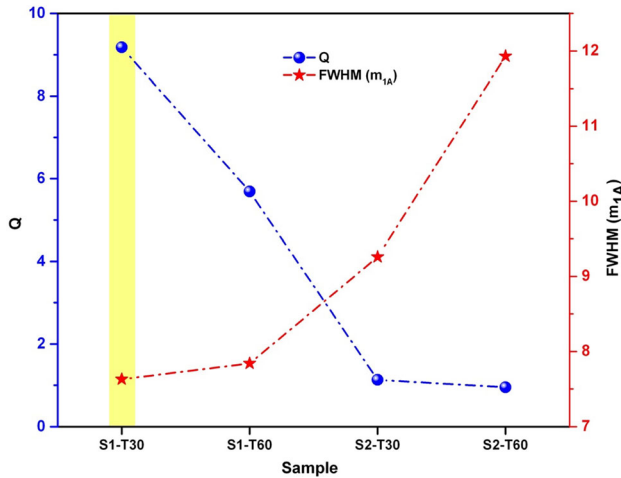


Fig. 5 Variation in the Q-factor and FWHM as a function of stack sequence and sulfurization time

reducing structural ordering for other samples were corroborated with the compositional inhomogeneity. SEM micrographs suggested the uniform particle growth of the S1-T30 sample. Thin film sulfurized using T30 profile for S1 series resulted in improved crystallinity and optimum band gap of 1.47 eV, whereas the same temperature profile for S2 series suffered from poor crystallinity and impurity phases. This study suggests that utilizing the stack order SLG/ZnS/Sn/Cu along with an optimum temperature rate profile with 30 min of high-temperature sulfurization produces CZTS thin film free from binary and ternary sulfide phases, which will be suitable for solar photovoltaic application.

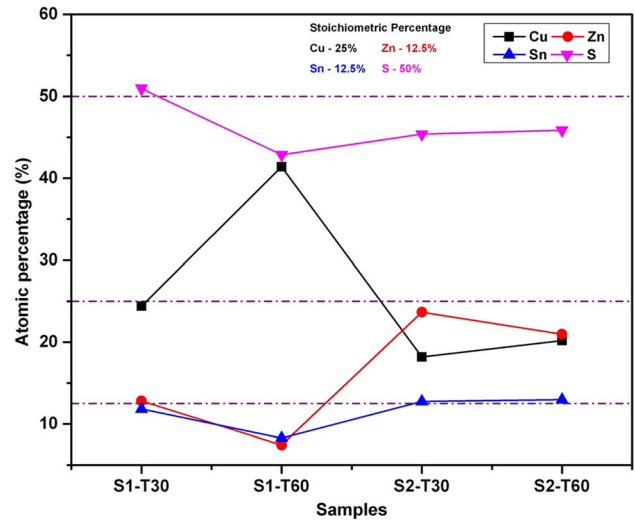


Fig. 6 Composition of CZTS thin films S1-T30, S1-T60, S2-T30, and S2-T60

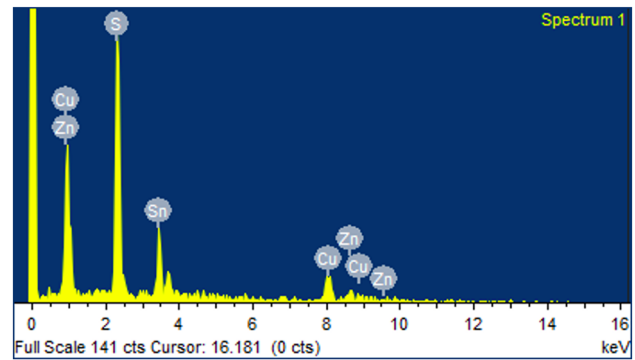


Fig. 7 EDS spectra of CZTS thin film of sample S1-T30

Table 3 Elemental composition of CZTS thin films of S1 series

Sample	Cu (25%)	Zn (12.5%)	Sn (12.5%)	S (50%)	$\frac{Cu}{(Zn+Sn)}$	$\frac{Zn}{Sn}$	$\frac{S}{(Cu+Zn+Sn)}$
S1-T30	24	13	12	51	0.96	1.08	1.04
S1-T60	41	7	8	43	2.73	0.88	0.77
S2-T30	18	24	13	45	0.49	1.85	0.82
S2-T60	20	21	13	46	0.59	1.62	0.85

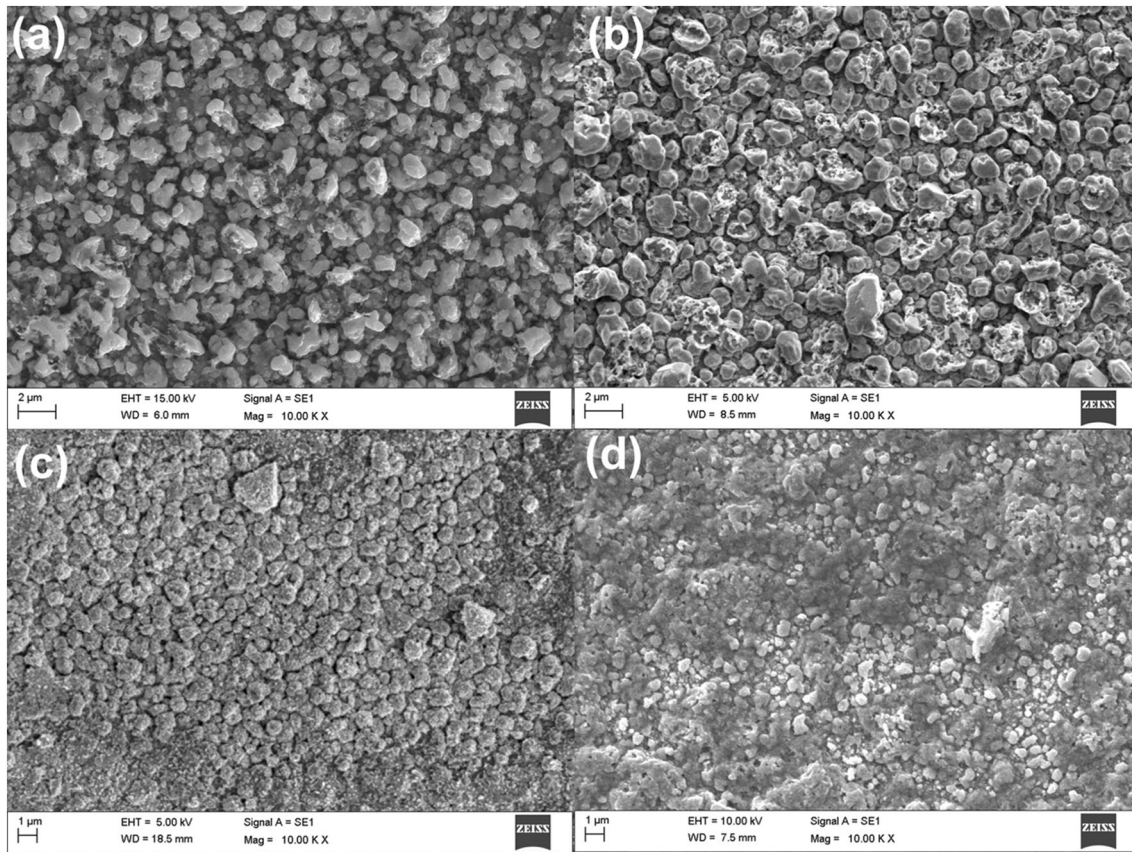


Fig. 8 SEM micrographs of **a** S1-T30, **b** S2-T60, **c** S2-T30, and **d** S2-T60 CZTS thin films

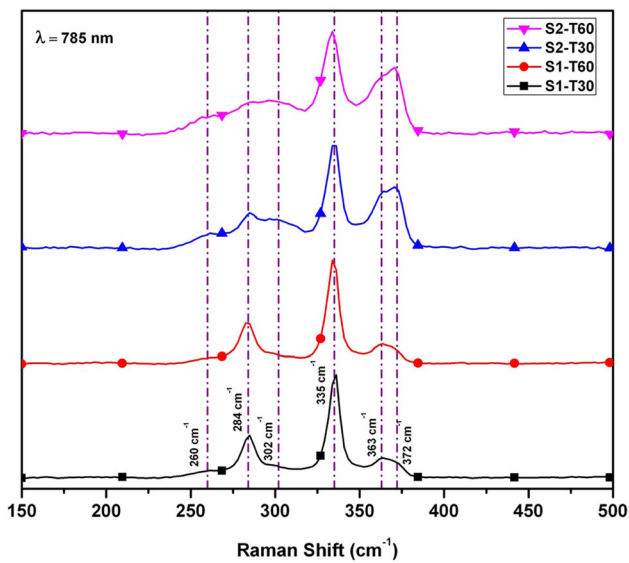


Fig. 9 Evolution of structural ordering of CZTS thin films as a function of stacking sequence and sulfurization time

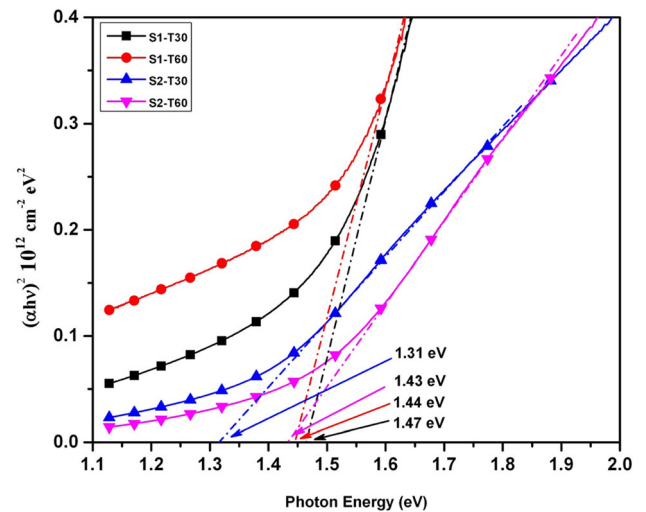


Fig. 10 The band gap of CZTS thin films obtained using the Tauc plot function

Acknowledgements

This work is executed with the support of the Extramural Research (EMR)/ Core Research Grant (CRG) project with sanction number DST-SERB/EMR/2017/002575 of the Science and Engineering Research Board (SERB), Department of Science and Technology (DST), Government of India.

Funding

Open access funding provided by Manipal Academy of Higher Education, Manipal.

Open Access This article is licensed under a Creative Commons Attribution 4.0 International License, which permits use, sharing, adaptation, distribution and reproduction in any medium or format, as long as you give appropriate credit to the original author(s) and the source, provide a link to the Creative Commons licence, and indicate if changes were made. The images or other third party material in this article are included in the article's Creative Commons licence, unless indicated otherwise in a credit line to the material. If material is not included in the article's Creative Commons licence and your intended use is not permitted by statutory regulation or exceeds the permitted use, you will need to obtain permission directly from the copyright holder. To view a copy of this licence, visit <http://creativecommons.org/licenses/by/4.0/>.

Data availability

The data pertaining to this report can be provided on a reasonable request.

References

- M.A. Green, Y. Hishikawa, E.D. Dunlop, D.H. Levi, J. Hohl-Ebinger, M. Yoshita, A.W.Y. Ho-Baillie, *Prog. Photovoltaics Res. Appl.* **27**, 3 (2019)
- S. Abermann, *Sol. Energy* **94**, 37 (2013)
- S. Delbos, *EPJ Photovoltaics* **3**, 35004 (2012)
- S. Giraldo, Z. Jehl, M. Placidi, V. Izquierdo-Roca, A. Pérez-Rodríguez, E. Saucedo, *Adv. Mater.* **31**, 1 (2019)
- L. Sun, H. Shen, H. Huang, A. Raza, Q. Zhao, J. Yang, *Vacuum* **165**, 186 (2019)
- T. Chandel, M.B. Zaman, S.K. Dwivedi, R. Poolla, *Vacuum* **159**, 341 (2019)
- N. Jnaneshwar, Y. Raviprakash, F. Bellarmine, M.S.R. Rao, R. Pinto, *Sol. Energy* **201**, 348 (2020)
- A. Fairbrother, L. Fourdrinier, X. Fontané, V. Izquierdo-Roca, M. Dimitrievska, A. Pérez-Rodríguez, E. Saucedo, *J. Phys. Chem. C* **118**, 17291 (2014)
- C.A. Meza Avendaño, N.R. Mathews, M. Pal, F.P. Delgado, X. Mathew, *ECS J. Solid State Sci. Technol.* **4**, P91 (2015)
- N. Thota, M. Gurubhaskar, M.A. Sunil, P. Prathap, Y.P.V. Subbaiah, A. Tiwari, *Appl. Surf. Sci.* **396**, 644 (2017)
- J. Lee, G. Han, J.H. Kim, *J. Korean Phys. Soc.* **75**, 735 (2019)
- Y.L. Zhou, W.H. Zhou, Y.F. Du, M. Li, S.X. Wu, *Mater. Lett.* **65**, 1535 (2011)
- K.S. Gour, A.K. Yadav, O.P. Singh, V.N. Singh, *Vacuum* **154**, 148 (2018)
- N.J. Choudhari, Y. Raviprakash, B.J. Fernandes, N.K. Udayashankar, *J. Alloys Compd.* **799**, 314 (2019)
- B. D. Cullity, *Elements of X-Ray Diffraction* (Addison-Wesley Publishing Company, Inc., 1956).
- P. Scherrer, *Math. Phys.* **2**, 98 (1918)
- B.T. Jheng, K.M. Huang, S.F. Chen, M.C. Wu, *Thin Solid Films* **564**, 345 (2014)
- P. Kalinauskas, E. Norkus, Z. Mockus, R. Giraitis, G. Stal-nionis, V. Jasulaitiene, R. Juškėnas, *J. Electrochem. Soc.* **167**, 026513 (2020)
- T. J. Whittles, in (Springer International Publishing, Cham, 2018), pp. C1–C1.
- A.-J. Cheng, M. Manno, A. Khare, C. Leighton, S.A. Campbell, E.S. Aydil, *J. Vac. Sci. Technol.* **29**, 051203 (2011)
- P.A. Fernandes, P.M.P. Salomé, A.F. da Cunha, *Thin Solid Films* **517**, 2519 (2009)
- Y. Zhang, J. Han, C. Liao, *CrystEngComm* **18**, 9026 (2016)
- M. Quennet, A. Ritscher, M. Lerch, B. Paulus, *J. Solid State Chem.* **250**, 140 (2017)
- J. Xu, J. Yang, S. Jiang, S. Shang, *Ceram. Int.* **47**, 4135 (2021)
- M. Dimitrievska, A. Fairbrother, X. Fontané, T. Jawhari, V. Izquierdo-Roca, E. Saucedo, A. Pérez-Rodríguez, *Appl. Phys. Lett.* **104**, 021901 (2014)
- J.J.S. Scragg, L. Choubrac, A. Lafond, T. Ericson, C. Platzer-Björkman, *Appl. Phys. Lett.* **104**, 41911 (2014)
- E.A. Davis, N.F. Mott, *Philos. Mag.* **22**, 903 (1970)
- J. Tauc, R. Grigorovici, A. Vancu, *Phys. Status Solidi* **15**, 627 (1966)

29. U. Chalapathi, S. Uthanna, V. Sundara Raja, Sol. Energy Mater. Sol. Cells **132**, 476 (2015)
30. G. Rey, A. Redinger, J. Sandler, T.P. Weiss, M. Thevenin, M. Guennou, B. El Adib, S. Siebentritt, Appl. Phys. Lett. **105**, 112106 (2014)

Publisher's Note Springer Nature remains neutral with regard to jurisdictional claims in published maps and institutional affiliations.